Auto-Calibration of Near-Field Microwave Measurements for Complex Permittivity Estimation

(Received 3 September 2025, Accepted 13 November 2025, Scheduled 16 December 2025)

Auto-Calibration of Near-Field Microwave Measurements for Complex Permittivity Estimation

Andrei Ludvig-Osipov, Simon Stenmark, Thomas Rylander*, and Tomas McKelvey

Department of Electrical Engineering, Chalmers University of Technology, SE-41296 Göteborg, Sweden

ABSTRACT: This paper presents a numerical study of a novel method for auto-calibration of scattering-parameter measurements in a near-field microwave sensor system. The here proposed method is applied to estimation of the average complex permittivity in a measurement domain from scattering parameters, corrupted by gain uncertainties in the measurement instruments. Simultaneously with the average complex permittivity, the gain uncertainties are also estimated. The characteristic property of the proposed method is that no simplified mathematical model of the measurement domain is assumed, and instead a set of a-priori calibrated observations is used. Numerical studies demonstrate the performance of the method in noiseless and noisy settings with and without nuisance stochastic perturbations in the measurement domain. An approach to compensate for the stochastic perturbations in the measurement domain permittivity is proposed, and it demonstrates an improved performance of the method in numerical examinations.

1. INTRODUCTION

An inseparable problem of microwave sensor and measurement systems is the decalibration, caused by drifts of parameters in a system [1, 2]. Calibration becomes a challenging task in particular in systems that operate in the near field, where simple mathematical models of electromagnetic interaction are typically unavailable [3, 4]. Calibration techniques that use calibration standards may suffer from non-ideal calibration standards which cause deviations in measurements [5]. Additionally in many practical uses, performing reference measurements for calibration during systems' operation is either infeasible or highly undesirable, and calibration performed simultaneously with measurements — so-called auto-calibration [6–10] — is preferable. The auto-calibration method proposed in this article addresses the calibration problem in such cases, while requiring calibrated measurements only on the systems' manufacturing stage. We consider average complex permittivity estimation in the measurement domain as an application example for the proposed method.

The microwave sensor systems operating in a near-field domain are key components in application areas ranging from healthcare [11, 12] to food industry [13] to automotive engines diagnostics [14]. A continuous drift of sensor parameters in these applications deems calibration performed separately from taking measurements unacceptable, as measurement errors gradually grow until calibration is repeated again. At the same time, calibration methods that continuously trace the parameter drift are inconvenient when a system is periodically kept idle or switched off. In some of the applications, such as in sensor systems inside automotive engines, no access to the measurement domain is available for performing a reference calibration.

The largest and most dynamic contribution to the drift of systems' parameters is typically due to phase and amplitude errors in sensors' amplifiers. The recent widespread availability of computational resources set a trend on compensating imperfections of low-cost hardware (sensors, amplifiers) by signal processing algorithms. This, while allowing to reduce the manufacturing costs of sensor systems, puts additional requirements on processing algorithms, among which calibration plays a crucial role and is essential for the correct operation. Such setup, however, allows us to identify the largest error contribution to be located in the sensors.

Complex permittivity estimation has a longstanding research history [15, 16] with a series of methods focusing on calibration-independent scattering-parameters measurements, see e.g., [17–20]. These methods rely on measurements of dielectric samples in a waveguide using a two-port setup, and require dielectric sample displacement, connection of removable waveguide sections or measurement of additional dielectric samples with different sizes. Another approach is to use a probe to measure the complex reflection coefficient of the material under test, which requires careful calibration of the measurement system [21]. Our proposed method, on the contrary, performs estimation from raw uncalibrated scattering parameters of a multiport without any additional manipulations.

The here proposed auto-calibration method operates with uncalibrated scattering-parameters of a multi-port sensor system. The a-priori knowledge, available to the method, is a (possibly approximate) mapping between the complex permittivity of the medium under test and the calibrated scattering parameters. From uncalibrated observations of scattering parameters, the method jointly estimates the unknown value of the parameter of interest and the complex amplification factors at the sen-

* Corresponding author: Thomas Rylander (rylander@chalmers.se).

sors. We validate and investigate the proposed method by numerical studies, where an estimation of a complex permittivity in a closed circular domain from uncalibrated scattering parameters is considered. Additionally, we consider an approach to compensate stochastic perturbations of the complex permittivity, also validated by numerical examples.

The rest of this article is organized as follows. In Section 2, the considered model of a sensor system is described, and the challenges related to calibration and stochastic perturbations in the system are identified. The auto-calibration method and the approach to compensate the stochastic perturbations are presented in Section 3. Numerical tests on an example application of complex-permittivity estimation for a stochastic medium in a circular cavity are given in Section 4. Section 5 summarizes and concludes the article.

2. MEASUREMENT SYSTEM MODEL AND AUTO-CALIBRATION PROBLEM

We consider a model of a near-field microwave measurement system that operates at a single frequency ω. The model is shown in Fig. 1 and consists of

- An N-port network Ω that includes the measurement domain with the medium under test and antennas with their feeding transmission lines terminated at the ports.
- N two-port microwave instruments $I_1, \ldots, I_N$, one for each port of the network Ω. The microwave instruments are connected with their measurement ports to the ports of the network Ω. This construction, terminated at the observer ports of the microwave instruments, constitutes an N-port network Θ.

In this paper, the considered medium under test is a dielectric medium in the measurement domain, and we aim to estimate

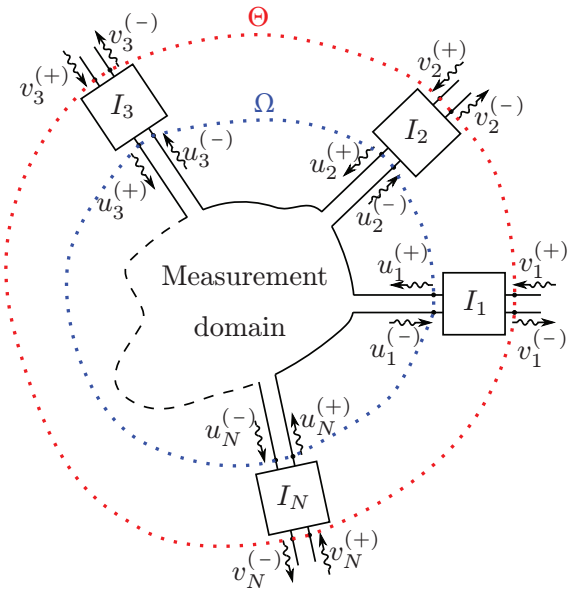

FIGURE 1. Near-field microwave measurement system with N ports. The p-th port is equipped with a two-port microwave instrument I_p, where $p = 1, \ldots, N$.

the average complex permittivity in the measurement domain. We only have access to the observer ports of Θ, while the microwave instruments $I_1, \ldots, I_N$ have unknown complex amplification factors. The goal of the auto-calibration algorithm is to, given observations of scattering parameters at the observer ports of Θ, compensate the unknown amplification factors and thus reconstruct the scattering parameters as seen at the ports of Ω. We assume that a-priori observations of the scattering parameters at the ports of Ω are available for a set of complex permittivity values of the medium under test. This set should cover the range at which we intend to estimate the complex permittivity from the observations of Θ.

2.1. Scattering-Parameter Model

The multiport Ω is associated with a scattering matrix $\mathbf{S}$ defined by its elements

$$S_{pq} = \left.\frac{u_p^{(-)}}{u_q^{(+)}}\right|_{u_r^{(+)}=0 \text{ for } r\neq q}, \tag{1}$$

where $(u_p^{(+)}, u_p^{(-)})$ are incident and reflected voltage amplitudes at the p-th port of Ω, see Fig. 1.

In a similar fashion, we introduce a data matrix $\mathbf{D}$ associated with the multiport Θ. The elements of the data matrix $\mathbf{D}$ are defined by

$$D_{pq} = \left.\frac{v_p^{(-)}}{v_q^{(+)}}\right|_{v_r^{(+)}=0 \text{ for } r\neq q} \tag{2}$$

where $(v_p^{(+)}, v_p^{(-)})$ are incident and reflected voltage amplitudes at the p-th port of Θ, see Fig. 1.

Each two-port microwave instrument I_p is described by a scattering matrix that relates its incident voltage amplitudes $u_p^{(-)}$ and $v_p^{(+)}$ to its reflected voltage amplitudes $u_p^{(+)}$ and $v_p^{(-)}$ according to

$$\begin{bmatrix} u_p^{(+)} \\ v_p^{(-)} \end{bmatrix} = \begin{bmatrix} 0 & t_p \\ r_p & 0 \end{bmatrix} \begin{bmatrix} u_p^{(-)} \\ v_p^{(+)} \end{bmatrix}, \tag{3}$$

where t_p, r_p are the complex-valued amplification factors on transmitting and receiving respectively. Here, we assume that (i) the instrument ports are impedance-matched such that reflections at the ports are negligible; and (ii) cross-talk between the instruments is negligible. These amplification factors, in addition to the amplification errors in the instruments, can model unknown imperfections in the transmission lines and antennas. In the following, we assume that the parameter drift is sufficiently slow for r_p and t_p to be considered quasi-stationary and, hence, constant during the auto-calibration process.

In the noise-free case, the scattering and data matrices are related as

$$\mathbf{D} = \mathbf{RST}, \tag{4}$$

where we have the unknown diagonal matrices

$$\mathbf{R} = \operatorname{diag}(r_1, r_2, \ldots, r_N) \text{ and} \tag{5}$$

$$\mathbf{T} = \operatorname{diag}(t_1, t_2, \ldots, t_N). \tag{6}$$

2.2. Noise Model

We assume the noise in the microwave instruments to be additive. The relation between the complex amplitudes (assembled here in vectors) $\mathbf{u}^{(\pm)} = (u_1^{(\pm)}, \ldots, u_N^{(\pm)})$ and $\mathbf{v}^{(\pm)} = (v_1^{(\pm)}, \ldots, v_N^{(\pm)})$ are

$$\begin{aligned} \mathbf{u}^{(+)} &= \mathbf{T}\mathbf{v}^{(+)} + \mathbf{n}^{(+)} \\ \mathbf{v}^{(-)} &= \mathbf{R}\mathbf{u}^{(-)} + \mathbf{n}^{(-)}. \end{aligned}$$

Here the noise voltage vectors $\mathbf{n}^{(+)}$ and $\mathbf{n}^{(-)}$ are complex random variables with a zero mean. Then, we have

$$\mathbf{v}^{(-)} = \mathbf{D}\mathbf{v}^{(+)} + \mathbf{R}\mathbf{S}\mathbf{n}^{(+)} + \mathbf{n}^{(-)}.$$

We get the data matrix $\tilde{\mathbf{D}}$ subject to noise associated with the microwave instruments as

$$\tilde{\mathbf{D}} = \mathbf{D} + \mathbf{R}\mathbf{S}\mathbf{N}^{(+)} + \mathbf{N}^{(-)}, \tag{7}$$

where $\mathbf{N}^{(+)}$ and $\mathbf{N}^{(-)}$ are noise voltage matrices with columns $\mathbf{n}^{(+)}$ and $\mathbf{n}^{(-)}$ associated with different realizations and normalized to the incident amplitudes $\mathbf{v}^{(+)}$.

2.3. Measurement-Domain Parametrization

The scattering parameters of the multiport Ω depend on the dielectric properties of the medium under test. The dielectric medium is characterized by the complex permittivity $\epsilon(\vec{r})$, where we refer to a particular realization of $\epsilon(\vec{r})$ as a permittivity profile. The dielectric medium is assumed to be linear and isotropic. Since the proposed method is applied to a single frequency, it allows for dispersive media. Hence, we consider the scattering parameter matrix to be a deterministic function $\mathbf{S}(\epsilon)$ of a measurement-domain permittivity profile $\epsilon(\vec{r}) \in \mathcal{E}$. The set $\mathcal{E}$ includes all the measurement-domain permittivity profiles that support a solution to Maxwell's equations.

2.4. Problem Formulation

Let the function $\mathbf{S}(\epsilon)$ be known on a subset $\mathcal{E}_0 \subset \mathcal{E}$ that contains only homogeneous permittivity profiles $\epsilon(\vec{r}) = \bar{\epsilon}$. An unknown homogeneous permittivity $\bar{\epsilon} \in \mathcal{E}_0$ is altered by an inhomogeneous stochastic perturbation $\delta\epsilon(\vec{r})$ such that $(\bar{\epsilon} + \delta\epsilon) \in \mathcal{E}$.

We work with K samples $\tilde{\mathbf{D}}^{(k)}$ (indexed by $k = 1, \ldots, K$) that depend on (i) the constant amplification-factor matrices $\mathbf{R}$ and $\mathbf{T}$, unperturbed permittivity $\bar{\epsilon}$ and (ii) different realizations of stochastic perturbations $\delta\epsilon$ of the permittivity profile together with the noise $\mathbf{N}^{(+)}$ and $\mathbf{N}^{(-)}$:

$$\tilde{\mathbf{D}}^{(k)} = \mathbf{R}\mathbf{S}(\bar{\epsilon} + \delta\epsilon^{(k)})\mathbf{T} + \mathbf{R}\mathbf{S}(\bar{\epsilon} + \delta\epsilon^{(k)})\mathbf{N}^{(+,k)} + \mathbf{N}^{(-,k)} \tag{8}$$

Given the samples $\tilde{\mathbf{D}}^{(k)}$, we wish to jointly estimate

1) the unknown homogeneous permittivity $\bar{\epsilon} \in \mathcal{E}_0$ and
2) the amplification-factor matrices $\mathbf{R}$ and $\mathbf{T}$.

The stochastic model of the perturbation $\delta\epsilon$ is application-specific. Reasonable assumptions here include $\mathrm{E}\{\delta\epsilon(\vec{r})\} = 0$ and a finite point-wise variance of $\delta\epsilon$. The operator $\mathrm{E}\{\cdot\}$ denotes the expectation of a random variable.

As evident from (8), the estimation problem has two noise contributions: the additive noise, as given in (7), and the stochastic permittivity perturbations $\delta\epsilon$, that equivalently can be seen as noise. In this paper, we focus on the latter contribution and hence consider the low additive noise scenarios.

2.4.1. Identifiability in $\mathbf{R}, \mathbf{T}$

It is not possible to uniquely determine $\mathbf{R}$ and $\mathbf{T}$ since $\mathbf{RST} = \tilde{\mathbf{R}}\mathbf{S}\tilde{\mathbf{T}}$ for the case $\tilde{\mathbf{R}} = \xi\mathbf{R}$, $\tilde{\mathbf{T}} = \xi^{-1}\mathbf{T}$ for any complex scalar $\xi \neq 0$. Here, ξ represents a (simultaneous) change in both magnitude and phase for the amplification factors (r_p, t_p) of all the instruments I_p. However, in many applications it is not necessary to know ξ in order to infer the quantities of interest that describe the medium under test. In the rest of the paper we assume $r_1 = 1$ to resolve this ambiguity.

Here, we wish to determine $(2N - 1)$ unknowns in $\mathbf{R}$ and $\mathbf{T}$. Given that the electromagnetic field problem in Ω fulfills reciprocity, we require at least that

- $N \geq 3$ if all (unique) scattering parameters are used to give $N(N+1)/2$ equations, and
- $N \geq 5$ if all (unique) transmission parameters are used to give $N(N-1)/2$ equations.

2.4.2. Identifiability in ϵ

We refer to the problem as identifiable in set $\mathcal{E}_0$ if the data equality $\mathbf{S}(\bar{\epsilon}_1) = \tilde{\mathbf{R}}\mathbf{S}(\bar{\epsilon}_2)\tilde{\mathbf{T}}$ holds only if $\bar{\epsilon}_1 = \bar{\epsilon}_2$ for some diagonal matrices $\tilde{\mathbf{R}}$, $\tilde{\mathbf{T}}$.

3. METHOD

The approach proposed here utilizes the diagonal structure of amplification matrices $\mathbf{R}$, $\mathbf{T}$, and the function $\mathbf{S}(\epsilon)$ is known for $\epsilon \in \mathcal{E}_0$. We attempt to calibrate the data matrix $\mathbf{D}$ so that it fits one of the known values of the scattering matrix $\mathbf{S}(\epsilon)$. This is performed by solving the following optimization problem

$$\hat{\epsilon} = \underset{\epsilon \in \mathcal{E}_0}{\operatorname{argmin}}\, g(\epsilon) \tag{9}$$

$$g(\epsilon) = \min_{\mathfrak{R}, \mathfrak{T} \in \mathcal{D}} ||\mathbf{S}(\epsilon) - < \mathfrak{R}\tilde{\mathbf{D}}\mathfrak{T} > ||_{\mathrm{F}}^2, \tag{10}$$

where $\mathcal{D}$ denotes the diagonal matrices, and $< \cdot >$ denotes a sample average, which is applied to the sequence of the realizations (w.r.t. perturbation $\delta\epsilon$ and the noise) of the modified data matrix $\mathfrak{R}\tilde{\mathbf{D}}\mathfrak{T}$. $||.||_{\mathrm{F}}$ denotes the Frobenius norm. For the case when only transmission parameters are used, the diagonal elements of $\mathbf{S}$ and $\tilde{\mathbf{D}}$ are set to zero.

The inner optimization problem (10) performs the autocalibration given a particular value of the permittivity profile $\epsilon \in \mathcal{E}_0$. The diagonal matrices $\mathfrak{R}$ and $\mathfrak{T}$ are used to compensate for the amplification matrices $\mathbf{R}$ and $\mathbf{T}$.

In the outer optimization problem (9), we estimate the permittivity profile $\hat{\epsilon}$ that belongs to the domain $\mathcal{E}_0$, which is typically approximated by a set of grid points that resolves the domain of interest sufficiently well. In such cases, Eq. (9) amounts to a search in $\mathcal{E}_0$ given the objective function $g(\epsilon)$.

The solution $\{\hat{\epsilon}, \hat{\mathbf{R}} = \mathfrak{R}^{-1}, \hat{\mathbf{T}} = \mathfrak{T}^{-1}\}$ to the joint parameter estimation and calibration problem (9)–(10) minimizes the misfit $||\mathbf{S}(\epsilon) - < \mathfrak{R}\tilde{\mathbf{D}}\mathfrak{T} > ||_{\mathrm{F}}^2$. The estimates are ideal when

the noise matrices $\mathbf{N}^{(+)}$, $\mathbf{N}^{(-)}$ and the perturbations $||\delta\epsilon||$ tend to zero and the problem is identifiable (see Section 2.4.2).

3.1. Averaging Operators

Here, we consider averaging operators suitable for $< \mathfrak{R}\tilde{\mathbf{D}}\mathfrak{T} >$ in (10). We denote $\mathfrak{R}\tilde{\mathbf{D}}\mathfrak{T}$ as $\tilde{\mathbf{S}}$, and the individual realizations by superscript as $\tilde{\mathbf{S}}^{(k)}$.

3.1.1. Arithmetic Average

We use the arithmetic average of the individual scattering parameters as

$$< \tilde{S}_{pq} >_{\text{aa}} = \frac{1}{K}\sum_{k=1}^{K} \tilde{S}_{pq}^{(k)} \tag{11}$$

where we have K samples that are indexed by $k = 1, \ldots, K$.

3.1.2. Generalized Average

For the cases when $\mathrm{E}\{\mathbf{S}(\bar{\epsilon} + \delta\epsilon)\} \neq \mathbf{S}(\mathrm{E}\{\bar{\epsilon} + \delta\epsilon\})$ the arithmetic average provides a biased estimate of the unperturbed scattering matrix. In this case, the space $\mathcal{E}_0$ can be used as a proxy for averaging:

$$< \tilde{S}_{pq} >_{\text{ga}} = S_{pq}\left(\frac{1}{K}\sum_{k=1}^{K} S_{pq}^{-1}\left(\tilde{S}_{pq}^{(k)}\right)\right). \tag{12}$$

Here, the functions $S_{pq} : \mathcal{E}_0 \to \mathbb{C}$ denote the pq-components of the matrix-valued function $\mathbf{S}(\cdot)$ and and $S_{pq}^{-1} : \mathbb{C} \to \mathcal{E}_0$ are the corresponding inverse functions. The inverse of an isolated component $S_{pq}(\cdot)$ can be uniquely determined only in a local neighbourhood of some permittivity value $\epsilon \in \mathcal{E}_0$. For the samples $\tilde{S}_{pq}^{(k)}$ corresponding to inhomogeneous perturbations, we apply a heuristic, according to which the function S_{pq}^{-1} assigns a homogeneous permittivity for the averaging. The point of operation, which determines the local neighbourhood where S_{pq}^{-1} is evaluated and chosen in connection with the optimization problem (10) to be the argument ϵ of $g(\epsilon)$.

3.2. Solving the Auto-Calibration Problem

The combined optimization problem (9), (10)

$$\hat{\epsilon}, \hat{\mathfrak{R}}, \hat{\mathfrak{T}} = \underset{\epsilon\in\mathcal{E}_0, \mathfrak{R}, \mathfrak{T}\in\mathcal{D}}{\operatorname{argmin}} \; ||\mathbf{S}(\epsilon) - < \mathfrak{R}\tilde{\mathbf{D}}\mathfrak{T} >_{\text{ga}} ||_{\text{F}}^2 \tag{13}$$

is in general non-convex in ϵ. For an efficient search for the global minimum, we propose a two-step optimization process: (i) computing *initial estimates* of $g(\epsilon)$, see Eq. (10), on a finite grid in $\mathcal{E}_0$ using *arithmetic average* and *alternating-least-squares calibrator*; and (ii) optimizing (13) starting from the *initial estimate* with lowest misfit $||\mathbf{S}(\epsilon) - < \mathfrak{R}\tilde{\mathbf{D}}\mathfrak{T} >_{\text{aa}} ||_{\text{F}}^2$ using *generalized average* and a general-purpose nonlinear-least-squares optimizer.

3.2.1. Initial Estimate Using Alternating-least-Squares Calibrator

For the initial estimate, we solve (10) for ϵ on the grid, resolving $\mathcal{E}_0$ sufficiently well. Moreover, the arithmetic average is used, which allows $< \mathfrak{R}\tilde{\mathbf{D}}\mathfrak{T} >_{\text{aa}} = \mathfrak{R} < \tilde{\mathbf{D}} >_{\text{aa}} \mathfrak{T}$. The optimization problem (10) in this case becomes a linear-least-squares problem in $\mathfrak{R}$ when $\mathfrak{T}$ is fixed and vice versa. This and a diagonal structure of $\mathfrak{R}, \mathfrak{T}$ allow for an efficient optimization approach, that alternates between optimizations with respect to $\mathfrak{R}$ and with respect to $\mathfrak{T}$.

The alternating-least-squares estimator operates as follows. If the data matrix $\bar{\mathbf{D}} = < \tilde{\mathbf{D}} >_{\text{aa}}$ is subject to measurement errors, a possible estimator is to minimize the sum of the squared errors between the model and the measurements. This can be formulated as minimizing the loss function

$$L(\mathfrak{R}, \mathfrak{T}) = \|\mathbf{S} - \mathfrak{R}\bar{\mathbf{D}}\mathfrak{T}\|_{\text{F}}^2 \tag{14}$$

From the diagonal structure of $\mathfrak{R}$ and $\mathfrak{T}$, it is easy to see that

$$\begin{aligned} L(\mathfrak{R}, \mathfrak{T}) &= \sum_{i=1}^{N} \|\mathbf{S}_{\bullet,i} - (\mathfrak{R}\bar{\mathbf{D}})_{\bullet,i}\mathfrak{T}_{ii}\|_{\text{F}}^2 \\ &= \sum_{i=1}^{N} \|\mathbf{S}_{i,\bullet} - \mathfrak{R}_{ii}(\bar{\mathbf{D}}\mathfrak{T})_{i,\bullet}\|_{\text{F}}^2. \end{aligned} \tag{15}$$

Here, the subscript notations $\mathbf{S}_{\bullet,i}$ and $\mathbf{S}_{i,\bullet}$ are used to represent respectively the i-th column and row of a matrix. With $\mathfrak{R}$ fixed, the minimizing argument of (15) is given by

$$\hat{\mathfrak{T}}_{ii} = \frac{(\mathfrak{R}\bar{\mathbf{D}})_{\bullet,i}^H \mathbf{S}_{\bullet,i}}{(\mathfrak{R}\bar{\mathbf{D}})_{\bullet,i}^H (\mathfrak{R}\bar{\mathbf{D}})_{\bullet,i}}, \quad i = 1, \ldots, N \tag{16}$$

and when $\mathfrak{T}$ fixed, the minimizing argument of (15) is

$$\hat{\mathfrak{R}}_{ii} = \frac{\mathbf{S}_{i,\bullet}(\bar{\mathbf{D}}\mathfrak{T})_{i,\bullet}^H}{(\bar{\mathbf{D}}\mathfrak{T})_{i,\bullet}(\bar{\mathbf{D}}\mathfrak{T})_{i,\bullet}^H}, \quad i = 1, \ldots, N \tag{17}$$

Here, the superscript $(.)^H$ denotes the Hermitian transpose.

In an attempt to minimize (14), we can employ the alternating least-squares method by iterating between (16) and (17).

1) Initialize $\mathfrak{T}$ and $\mathfrak{R}$ with unit diagonal entries
2) Solve (16) for $\mathfrak{T}$ with fixed $\mathfrak{R}$
3) Solve (17) for $\mathfrak{R}$ with fixed $\mathfrak{T}$
4) Assess the residual:
   - Go back to step 2 if the change in the residual is larger than the tolerance set by the user
   - Otherwise, stop iterating and accept $\mathfrak{T}$ and $\mathfrak{R}$ as an approximate solution.

Note that in this article, we consider low additive noise levels. For the cases with high levels of the additive noise, the data matrix $\bar{\mathbf{D}}$ (and hence the additive noise) enter expressions (16)–(17) nonlinearly. This may result in large calibration errors. There, the minimization of a loss function $\|\bar{\mathbf{D}} - \mathbf{RST}\|_{\text{F}}^2$ with

respect to $\mathbf{R}, \mathbf{T}$ can be performed and heuristically accepted as an approximate solution to (10). In the minimization of $\|\bar{\mathbf{D}} - \mathbf{RST}\|_{\mathrm{F}}^2$ using the alternating least squares, the additive noise enters linearly in the counterparts of expressions (16)–(17).

3.2.2. Refined Estimate with Nonlinear Least Square Estimator

After applying the alternating-least-squares estimator to all permittivity values ϵ on the grid (a finite subset of $\mathcal{E}_0$), the permittivity value giving the smallest residual (14) and its estimates of $\mathbf{R}$, $\mathbf{T}$ are picked as initial values for the optimization problem (13). This problem is consequently solved by a general-purpose optimizer (e.g., nonlinear least squares) with generalized-average operator to obtain the final estimates $\hat{\epsilon}, \hat{\mathfrak{R}} = \hat{\mathbf{R}}^{-1}, \hat{\mathfrak{T}} = \hat{\mathbf{T}}^{-1}$. This optimization is performed over a continuous set $\mathcal{E}_0$, where $\mathbf{S}(\epsilon)$ is interpolated between the grid points. We use Möbius transformations for the interpolation, as discussed in the following section.

3.3. Local Approximation Functions

Within the permittivity estimation problem, a suitable class of local approximation functions are Möbius transformations. We use the Möbius transformations (i) to interpolate $\mathbf{S}(\epsilon)$ between the grid points in the permittivity estimation problem, see Section 3.2.2 and (ii) to compute a generalized average, see Section 3.1.2. The Möbius transformations can be seen as reduced-order Padé approximants. For a homogeneous permittivity ϵ that can be represented by a complex scalar, a Padé approximation is

$$S_{pq}(\epsilon) \simeq \sum_m \frac{r_{pq,m}}{\epsilon - \epsilon_m}. \tag{18}$$

Here, $r_{pq,m}$ denote residues, and ϵ_m denote complex poles in the ϵ-space. In the proximity of a pole ϵ_n, the variation of the corresponding n-th term is dominant, and hence the residue-pole representation can be further reduced to

$$\begin{aligned} S_{pq}(\epsilon) &\simeq C_{pq,n} + \frac{r_{pq,n}}{\epsilon - \epsilon_n} \\ &= \frac{(-C_{pq,n}/\epsilon_n)\epsilon + (-C_{pq,n} - r_{pq,n}/\epsilon_n)}{(-1/\epsilon_n)\epsilon + 1} \\ &= \frac{\alpha\epsilon + \beta}{\gamma\epsilon + 1} \triangleq M(\epsilon), \end{aligned} \tag{19}$$

where we assume that

$$C_{pq,n} = \sum_{m \neq n} \frac{r_{pq,m}}{\epsilon - \epsilon_m} \tag{20}$$

is approximately a constant. One advantage of the Möbius transformation as an approximation function is the simplicity of its inverse

$$M^{-1}(S_{pq}) = \frac{S_{pq} - \beta}{-\gamma S_{pq} + \alpha}. \tag{21}$$

In practice, parameters α, β, and γ are determined by a least-squares fit of the scattering parameters to its Möbius approximations in a neighborhood of some permittivity value. That is, for every scattering matrix component $S_{pq}(\epsilon)$ we look for a Möbius transformation $M_{pq}(\epsilon)$ parametrized by $\alpha_{pq}, \beta_{pq}, \gamma_{pq}$:

$$\begin{aligned} &\{\alpha_{pq}, \beta_{pq}, \gamma_{pq}\} \\ &= \operatorname*{argmin}_{\alpha_{pq},\beta_{pq},\gamma_{pq}\in\mathbb{C}} \sum_i |S_{pq}(\epsilon_i) - M_{pq}(\epsilon_i)|^2 \\ &= \operatorname*{argmin}_{\alpha_{pq},\beta_{pq},\gamma_{pq}\in\mathbb{C}} \sum_i \left| S_{pq}(\epsilon_i) - \frac{\alpha_{pq}\epsilon_i + \beta_{pq}}{\gamma_{pq}\epsilon_i + 1} \right|^2. \end{aligned} \tag{22}$$

with a finite set of points $\epsilon_i \in \mathcal{E}_0$ taken in proximity of an approximation point. The optimization problem (22) is recasted as a linear least squares problem minimizing $\sum_i |S_{pq}(\epsilon_i)(\gamma_{pq}\epsilon_i + 1) - \alpha_{pq}\epsilon_i + \beta_{pq}|^2$.

4. NUMERICAL EXAMPLES

We consider auto-calibration for estimation of mean complex permittivity in an enclosed circular region.

4.1. Geometry

A two-dimensional circular measurement domain of radius 0.0301 m filled with a stochastic inhomogeneous complex permittivity $\epsilon(\vec{r}) = \epsilon'(\vec{r}) - j\epsilon''(\vec{r})$ is connected to $N = 6$ parallel-plate waveguides of width 0.0047 m and uniform permittivity $\epsilon_{\mathrm{wg}} = 38$, see an example in Fig. 2. This geometry models a type of microwave sensor system that is intended for an inhomogeneous dielectric medium that is transported through a metal pipe [22, 23]. Each waveguide is terminated with a measurement port of a corresponding microwave instrument. In all the numerical examples here, the frequency $\omega/2\pi$ is 2.5 GHz.

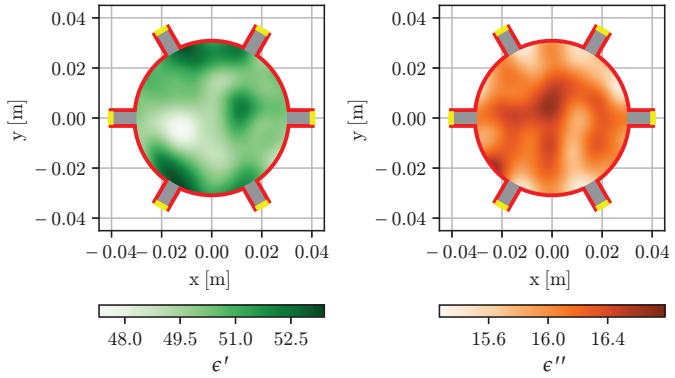

FIGURE 2. Example of the relative permittivity in the measurement domain Ω for $\mu' = 50$, $\sigma' = 1$, $\mu'' = 16$, $\sigma'' = 0.32$. PEC walls are in red, waveguides are in gray and waveguide ports are in yellow.

The real and imaginary parts of permittivity follow normal distributions $\epsilon'(\vec{r}) \sim \mathcal{N}(\mu', \sigma')$ and $\epsilon''(\vec{r}) \sim \mathcal{N}(\mu'', \sigma'')$ for every coordinate $\vec{r}$ in the measurement domain. Here, μ', σ', μ'', and σ'' are the expected values and standard deviations of the real and imaginary parts of the stochastic permittivity respectively. Their auto-covariances are given by

$$\operatorname{cov}[\epsilon'(\vec{r}), \epsilon'(\vec{r} + \delta\vec{r})] = (\sigma')^2 \exp\left(-\frac{|\delta\vec{r}|^2}{\varrho^2}\right), \tag{23}$$

$$\mathrm{cov}[\epsilon''(\vec{r}),\epsilon''(\vec{r}+\delta\vec{r})] = (\sigma'')^2 \exp\left(-\frac{|\delta\vec{r}|^2}{\varrho^2}\right). \quad (24)$$

where $\varrho = 0.01\,\mathrm{m}$ is the correlation length of the stochastic permittivity. We assume ϵ' and ϵ'' to be indepedent and hence $\mathrm{cov}[\epsilon'(\vec{r}),\epsilon''(\vec{r}+\delta\vec{r})] = 0$. The variance σ'' is normalized with respect to the expected values:

$$\sigma'' = \sigma' \frac{\mu''}{\mu'}. \quad (25)$$

In connection to the problem formulation in Section 2.4, the stochastic permittivity $\epsilon(\vec{r})$ here can be seen as a sum of a homogeneous permittivity $\bar{\epsilon} = \{\mu' - j\mu''\}$ and a stochastic non-zero inhomogeneous perturbation. All the homogeneous permittivities in this case belong to $\mathcal{E}_0$, while the perturbed ones are in $\mathcal{E}$.

4.2. Signal-to-Noise Ratio

By treating $\mathbf{D}$ in (7) as a signal and the rest of the terms $\{\mathbf{RSN}^{(+)} + \mathbf{N}^{(-)}\}$ as noise, we define the signal-to-noise ratio as

$$\mathrm{SNR} = \frac{||\mathbf{D}||_{\mathrm{F}}^2}{\mathrm{E}\{||\mathbf{RSN}^{(+)} + \mathbf{N}^{(-)}||_{\mathrm{F}}^2\}}. \quad (26)$$

Furthermore, in the numerical examples, we assume that all the microwave instruments contribute the same noise level, both on the receiving and transmitting. Hence, all the entries in $\mathbf{N}^{(+)}$ and $\mathbf{N}^{(-)}$ are independent normally distributed random variables with zero mean and variance σ_{N}^2. This assumption entails that the total noise level equates to

$$\begin{aligned} &\mathrm{E}\{||\mathbf{RSN}^{(+)} + \mathbf{N}^{(-)}||_{\mathrm{F}}^2\} \\ =\ &\mathrm{E}\{||\mathbf{RSN}^{(+)}||_{\mathrm{F}}^2\} + \mathrm{E}\{||\mathbf{N}^{(-)}||_{\mathrm{F}}^2\} \\ =\ &N||\mathbf{RS}||_{\mathrm{F}}^2\sigma_{\mathrm{N}}^2 + N^2\sigma_{\mathrm{N}}^2. \end{aligned} \quad (27)$$

To see that, consider

$$\begin{aligned} \mathrm{E}\{||\mathbf{RSN}^{(+)}||_{\mathrm{F}}^2\} &= \sum_{i=1}^{N}\sum_{j=1}^{N} \mathrm{E}\{|(\mathbf{RSN}^{(+)})_{ij}|^2\} \\ &= \sum_{i=1}^{N}\sum_{j=1}^{N} \mathrm{E}\left\{\left|\sum_{k=1}^{N}(\mathbf{RS})_{ik}\mathbf{N}_{kj}^{(+)}\right|^2\right\} \\ &= \sum_{i=1}^{N}\sum_{j=1}^{N}\sum_{k=1}^{N} |(\mathbf{RS})_{ik}|^2 \mathrm{E}\left\{|\mathbf{N}_{kj}^{(+)}|^2\right\} \\ &= N||\mathbf{RS}||_{\mathrm{F}}^2\sigma_{\mathrm{N}}^2, \end{aligned}$$

where the cross-terms in the summation over index k have vanished due to independence of random elements in matrix $\mathbf{N}^{(+)}$. The term in (27) associated with $\mathbf{N}^{(-)}$ is treated similarly, with $\mathbf{RS}$ replaced with the identity matrix.

The signal-to-noise ratio then becomes

$$\mathrm{SNR} = \frac{||\mathbf{RST}||_{\mathrm{F}}^2}{N\sigma_{\mathrm{N}}^2(N + ||\mathbf{RS}||_{\mathrm{F}}^2)}. \quad (28)$$

The signal-to-noise ratio (26), in the case of stochastic perturbations of the scattering matrix $\mathbf{S}(\bar{\epsilon}+\delta\epsilon)$ due to a stochastic $\delta\epsilon$, is computed with respect to the deterministic value $\mathbf{S}(\bar{\epsilon})$ with $\bar{\epsilon} \in \mathcal{E}_0$.

4.3. Amplification Matrices

The amplification matrices $\mathbf{R}, \mathbf{T}$ are diagonal with their elements being random variables with amplitude uniformly distributed in the range $[1, 2]$ and with phase uniformly distributed in the range $[0, 2\pi]$.

4.4. Error Assessment

To evaluate the accuracy of the estimate, the relative estimation error of the expected value of the permittivity $|\hat{\epsilon} - \bar{\epsilon}|/|\bar{\epsilon}|$ is considered.

The calibration accuracy is evaluated via

$$\frac{\sum_{p=1}^{N}\sum_{q=1}^{N} |\hat{\mathbf{R}}_{pp}\hat{\mathbf{T}}_{qq} - \mathbf{R}_{pp}\mathbf{T}_{qq}|^2}{\sum_{p=1}^{N}\sum_{q=1}^{N} |\mathbf{R}_{pp}\mathbf{T}_{qq}|^2}. \quad (29)$$

Note that this metric is invariant to the scalar ambiguity ξ, see Section 2.4.1.

4.5. Numerical Tests

4.5.1. Least-Square Estimator

The least-squares estimator (Section 3.2.1) has been used to solve the minimization problem (10), and the results are plotted in Fig. 3. In this example, the data matrix is $\mathbf{D} = \mathbf{RS}(\bar{\epsilon} = 60 - \mathrm{j}12)\mathbf{T}$, with $\mathbf{R}, \mathbf{T}$ unknown random amplification matrices of a diagonal form. A noise-free scenario $\sigma_{\mathrm{N}} = 0$ is considered in this case. Each point (ϵ', ϵ'') in Figs. 3(a), (c) correspond to testing the data matrix $\mathbf{D}$ against a hypothetical scattering matrix $\mathbf{S}(\epsilon' - \mathrm{j}\epsilon'')$ in the alternating-least-squares procedure, described in Section 3.2.1. Fig. 3(a) depicts the misfit (14) after the alternating-least-squares procedure, and Fig. 3(c) depicts the corresponding calibration error (29).

The cross-sections of the misfit (at dashed-dotted lines A, B in Fig. 3(a)) are shown in Fig. 3(b). Additionally, Fig. 3(b) contains the cross-sections for the cases, when the permittivity in the data matrix is perturbed according to Section 4.1 with the standard deviations of the real part of permittivity $\sigma' = \{2.5, 5.0\}$. The standard deviations of imaginary part of permittivity σ'' are given according to (25). In the cases of non-zero perturbations, an arithmetic average of the data matrix for 100 realizations of stochastic permittivity has been used.

This result demonstrates that the misfit is a non-convex function of the search permittivity variable (ϵ', ϵ'') with clearly pronounced global minimum, which needs to be taken into account when choosing an optimization method for (9)–(10). Presence of the permittivity perturbations in the data matrix $\mathbf{D}$ results in a shift of the minimum from the true permittivity value in the misfit, hence an approach to combat such a bias — the use of generalized average — needs to be used in such cases. From Fig. 3(c) we note that slight inaccuracies in the permittivity estimation lead to a drastic increase of the calibration error.

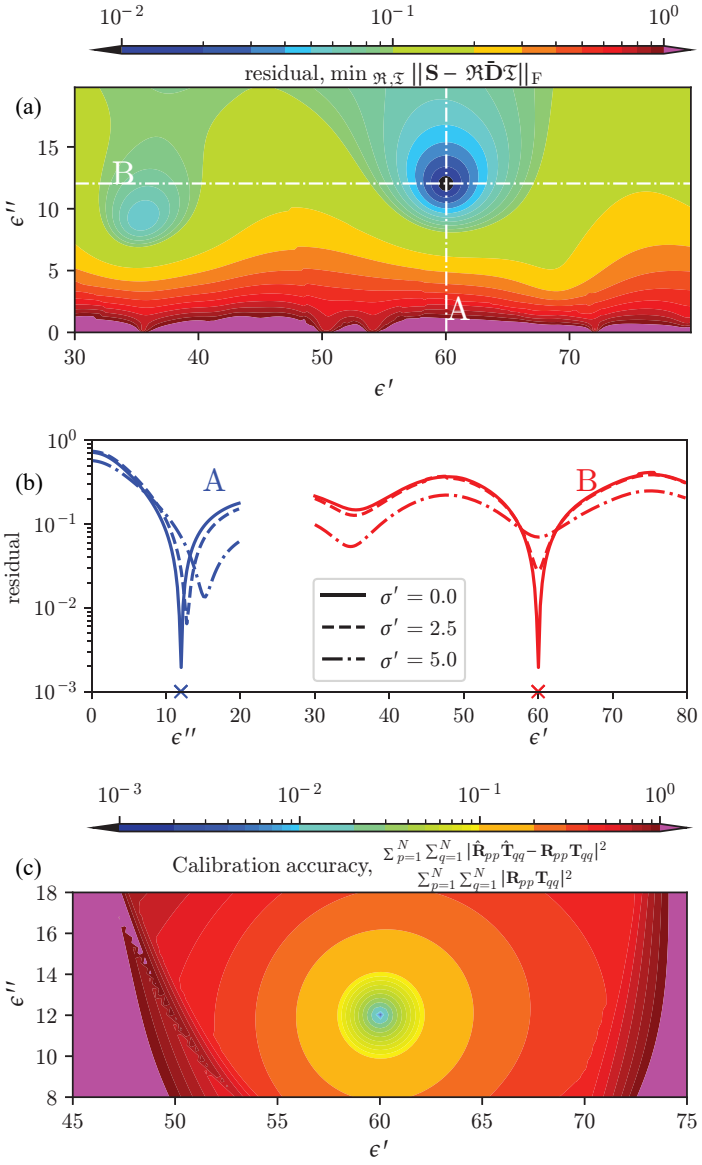

FIGURE 3. (a) Example of the calibrated misfit (14) as a function of a complex minimization variable $\epsilon = \epsilon' - \mathrm{j}\epsilon''$. The true permittivity value is $\bar{\epsilon} = 60 - \mathrm{j}12$, the observed sample corresponds to the uniform permittivity with random calibration error and frequency is 2.5 GHz. (b) Cross-sections of the colormap plot. Crosses on the horizontal axis show the true permittivity value. (c) Normalized calibration error as a function of the minimization variable.

4.5.2. Estimation and Calibration for Unperturbed Permittivities

The permittivity estimation and calibration errors of the proposed approach, described in Section 3.2, are plotted in Fig. 4. For each point in these graphs, a data matrix $\mathbf{D} = \mathbf{RS}(\bar{\epsilon} = \epsilon' - \mathrm{j}\epsilon'')\mathbf{T}$ is generated without noise and permittivity perturbations. First, the initial estimate of $\epsilon, \mathbf{R}, \mathbf{T}$ is obtained, using alternating-least-squares on a discrete permittivity grid with steps 0.31 both in ϵ' and in ϵ''. Then, the initial estimate is used to solve (13) with a general-purpose nonlinear-least-squares algorithm and a generalized average. The Möbius transformations, used for interpolation of $\mathcal{E}_0$ in the optimization over ϵ and for the generalized averages, are computed according to (22)

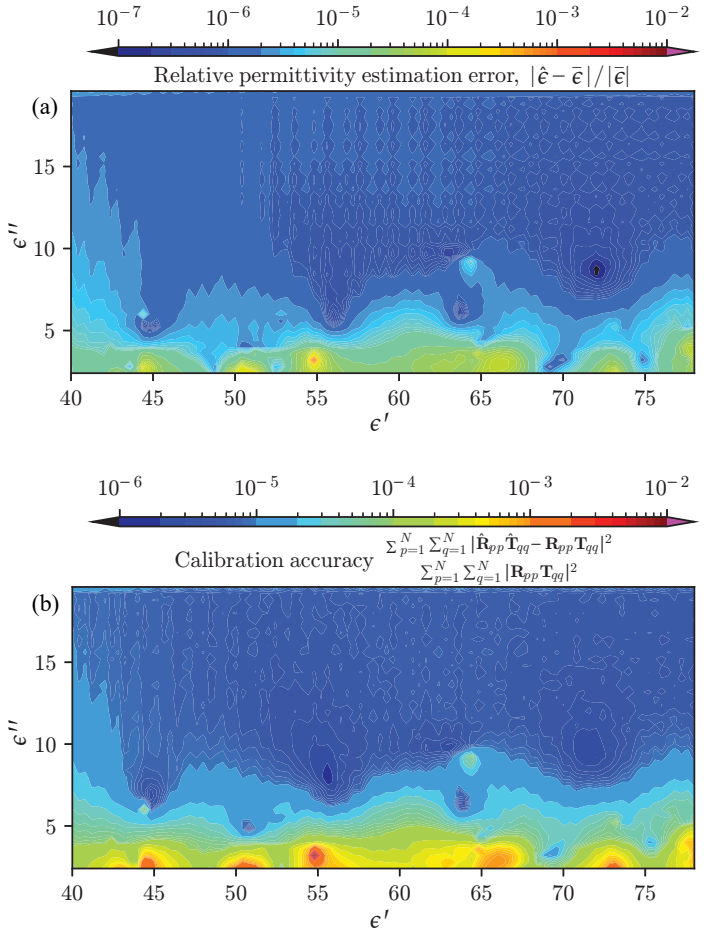

FIGURE 4. Normalized permittivity-estimation and calibration errors as functions of the true permittivity $\bar{\epsilon} = \bar{\epsilon}' - \mathrm{j}\bar{\epsilon}''$. The permittivity is homogeneous ($\sigma', \sigma'' = 0$) in the measurement domain, and no instrument noise is present.

with an approximation window of 5×5 grid points. The relative permittivity error, Fig. 4(a), and the calibration error, Fig. 4(b), are plotted as functions of the true permittivity $\bar{\epsilon} = \epsilon' - \mathrm{j}\epsilon''$. The results indicate that the method provides relative permittivity estimation error lower than 10^{-3} and calibration error lower than 10^{-2} for all considered true permittivity values. A somewhat lower accuracy in the low-loss region ($\epsilon'' < 5.0$) is related to a lower accuracy of approximation with Möbius transformations in that region. This numerical test indicates that permittivity is identifiable (as per Section 2.4.2) for the considered numerical example.

4.5.3. Additive Noise and Stochastic Permittivity

In Fig. 5, the dependence of estimation and calibration errors on standard deviation of permittivity is shown. The depicted curves are average performance over 100 Monte Carlo iterations. On each iteration, the estimation and calibration were performed using $K = 50$ realizations of the data matrix. The values of $\mathbf{R}$ and $\mathbf{T}$ are the same for all K realizations. The true mean permittivity is $\bar{\epsilon} = \{60.4 - \mathrm{j}13.2\}$, and two cases, with and without usage of reflection parameters of $\tilde{\mathbf{D}}$ in the autocalibration process, are considered. The generalized average

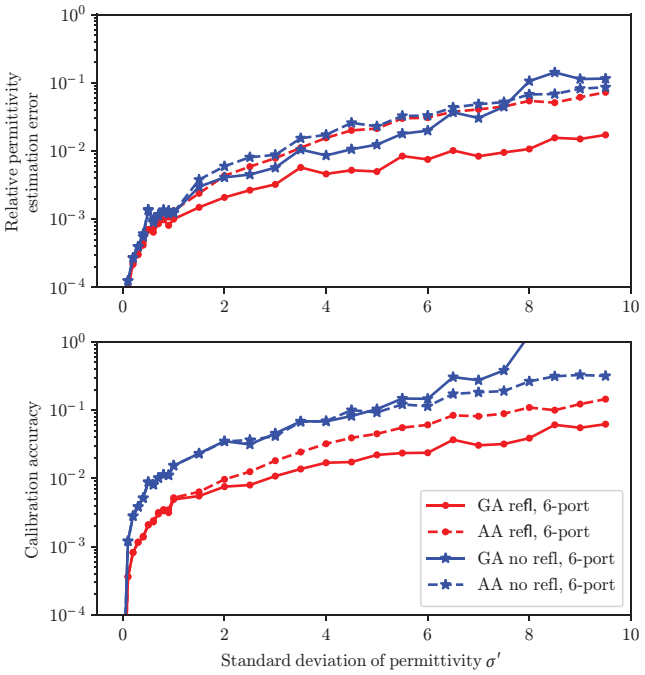

FIGURE 5. Normalized permittivity-estimation and calibration errors for true permittivity value $\bar{\epsilon} = 60.4 - \mathrm{j}13.2$ as a function of a standard deviation of permittivity.

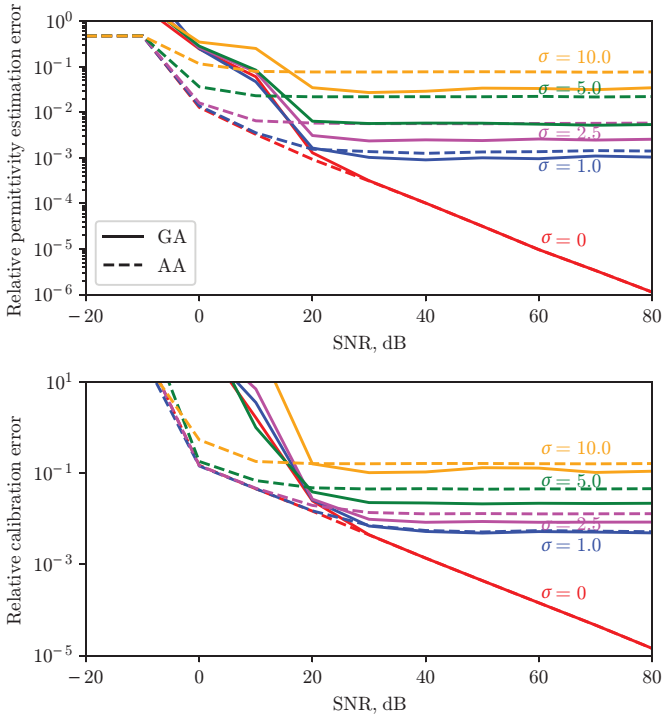

FIGURE 6. Normalized permittivity-estimation and calibration errors as functions of SNR for true permittivity value for $\bar{\epsilon} = 60.4 - \mathrm{j}13.2$ and a series of values of standard deviation of permittivity σ'. 6-port with reflection coefficient.

demonstrates an overall superior performance over the arithmetic average for the case when the reflection parameters are used. When the reflection parameters are not used, the permittivity estimation is better with the generalized average for

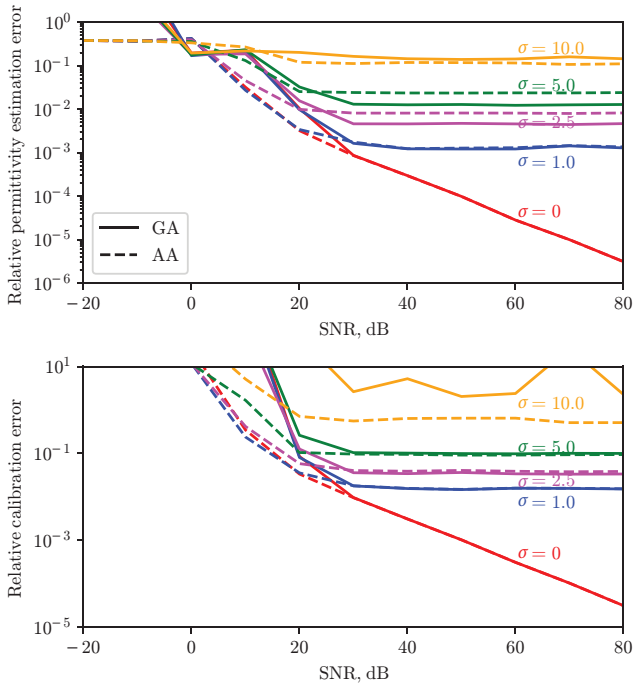

FIGURE 7. Normalized permittivity-estimation and calibration errors as functions of SNR for true permittivity value for $\bar{\epsilon} = 60.4 - \mathrm{j}13.2$ and a series of values of standard deviation of permittivity σ'. 6-port no reflection coefficient.

$\sigma' < 8$, while the calibration accuracy is similar with both averaging methods for $\sigma' \leq 6$.

Figures 6 and 7 show dependence of relative permittivity estimation and calibration errors as functions of signal-to-noise ratio respectively with and without the usage of reflection coefficient in the auto-calibration process. The noise has been added to the data matrices according to the model (7) and the signal-to-noise ratio is evaluated according to (28). In the high-SNR regime the performance agrees with the one that is observed in Fig. 5. The permittivity estimation and calibration errors saturate at SNR around 30 dB and above, which indicates that the stochastic components of permittivity act as an effective noise, which dominates at this SNR range.

5. DISCUSSION

Fully automatized online-monitoring of product quality is important in many process industries. In principle, the auto-calibration approach proposed in this article can be altered to estimate other measurement-domain parameters instead of or in combination with the mean permittivity, as long as the overall model of the measurement system follows (4) and the other prerequisites stated throughout the article are met. The microwave instruments I_p are assumed to be impedance-matched, and we assume that the crosstalk between instruments is negligible, which are standard issues to be addressed in the design of most microwave systems. To be able to identify the amplification matrices, the number of ports must be at least three if all (unique) scattering parameters are used and five if all (unique) transmission parameters are used, where a large number of ports may be challenging to fit for applications where space is lim-

ited. The question of identifiability for the parameters of interest is generally a complicated question in inverse scattering problems [24] and must be addressed for each new and unique application, where other issues such as ill-posedness also must be considered. It should be emphasized that the grid search on $\mathcal{E}_0$ provides a robust approach to the outer optimization problem (9), as long as the parameter domain of interest is properly resolved.

5.1. Computational Complexity

For an application with D_{g} parameters in (9) and a grid with $N_{\mathrm{g},i}$ grid points for the i-th parameter, the number of entries in the grid necessary to represent $\mathcal{E}_0$ is $N_{\mathrm{g,tot}} = \prod_{i=1}^{D_{\mathrm{g}}} N_{\mathrm{g},i}$. Depending on application, this may imply major memory requirements and possible alternatives are discussed in Section 5.3.

For each grid point, the alternating-least-squares calibrator in Section 3.2.1 is applied, which involves $\mathcal{O}(N^2)$ floating-point operations (flops) per iteration. The number of iterations required for convergence is denoted N_{it}. Thus, the computational complexity of determining the initial estimate of the solution $\{\hat{\epsilon}, \hat{\mathbf{R}} = \mathfrak{R}^{-1}, \hat{\mathbf{T}} = \mathfrak{T}^{-1}\}$ is $\mathcal{O}(N_{\mathrm{g,tot}} N_{\mathrm{it}} N^2)$. To refine this initial estimate, a nonlinear least square estimator is applied as discussed in Section 3.2.2. Typically, the initial estimate is sufficiently close to the sought optimum to make a nonlinear least-squares estimator converge in a few iterations and, in addition, this estimator only needs to be applied once (i.e., not for all grid points). Thus, the computational cost for this last step is expected to be negligible as compared to the determination of the initial estimate. In conclusion, the overall computational complexity in terms of flops is $\mathcal{O}(N_{\mathrm{g,tot}} N_{\mathrm{it}} N^2)$ and the memory requirements scale as $\mathcal{O}(N_{\mathrm{g,tot}})$. Since the alternating-least-squares is applied independently for each grid point, the grid-search is massively parallelizable which makes it attractive for implementation on specialized hardware such as a graphics processing unit (GPU). Moreover, in applications where the calibration and material parameters drift slowly in comparison to the time required to perform an estimation, the outer optimization problem (9) can use the previous solution as a good initial guess, which presents the opportunity for a significant reduction in overall computational cost.

5.2. Comparison with Other Methods

There are many well-known calibration techniques, such as TRL (Though-Reflect-Line) [25] and SOLT (Short-Open-Load-Through) [26], that assume that the measurement setup can be modified during calibration. For calibration procedures performed offline at scheduled intervals, measurement system issues may remain undetected until the next calibration, potentially compromising product quality. This article aims at applications that require online calibration concurrently with the intended material estimation and, thus, offline calibration methods are considered unattractive or impossible to use.

Estimation methods in the literature typically require special conditions to be fulfilled, such as the Nicolson-Ross-Weir algorithm [27, 28] that require that the material under test is a planar material slab (in combination with that the material is linear, isotropic and homogeneous). Other estimation methods provide useful information on the relation between the material parameters and the observed scattered field but typically at the expense of simplifying assumptions such as electrically small problems [29] or impenetrable scatterers [30]. Again, such estimation algorithms can rarely be directly used in industrial applications that typically feature complicated geometries, inhomogeneous media, large contrasts and other circumstances that are not compatible with the prerequisites of such specialized methods.

5.3. Extensions and Future Work

Some applications may require broad frequency-band data for a successful material estimation and sensor calibration. In such cases, the sensor system must operate over a large frequency-band, where ultra wide-band (UWB) antennas may be a crucial component [31, 32].

For high-dimensional problems in terms of permittivity and/or other parameters, it can be prohibitively expensive to create, store, and use a set of a-priori observations for the entire parameter domain $\mathcal{E}_0$ in terms of computational resources and/or memory requirements. Here, an attractive alternative is to train and use a computationally efficient surrogate model [33] for the mapping from $\mathcal{E}_0$ to the scattering parameters, where some alternatives are (i) deep neural networks [34, 35] and (ii) polynomial-based surrogate models [36]. Such surrogate models can also account for frequency variations, which may be important in wide frequency-band applications. Moreover, a surrogate model that is not restricted to a grid eliminates the need for local interpolation functions. However, since the generalized average (12) exploits the inverse S_{pq}^{-1}, it is desirable that the surrogate model is at least locally invertible. Here, one possible approach is to exploit invertible surrogate models such as invertible neural networks [37, 38]. Equipped with powerful surrogate models to represent mapping from $\mathcal{E}_0$ to the scattering parameters, it may be possible to approach applications with more complicated constitutive relations for the media involved such as dispersive and anisotropic [39, 40] media, which would require more parameters to represent the constitutive relation.

6. CONCLUSION

In this article, a method for auto-calibration of a multiport sensor system is presented. The method is independent of the sensor system geometry and operates with scattering-parameter observations. It jointly calibrates the scattering parameters and estimates the average complex permittivity in the measurement domain. For the operation of the method, a-priori calibrated observations for a set of the permittivity values are required. This set of observations should cover the permittivity space to a desired accuracy. The only assumptions of the method are that the calibration error follows the model (4), and that the identifiability conditions are satisfied.

The proposed method has demonstrated good calibration and mean-permittivity-estimation accuracies for all values of the permittivity region considered in the numerical studies, where

a complex-permittivity estimation in a cylindrical region has been considered. The non-uniformity of estimation and calibration errors in the complex-permittivity domain indicates that the proposed method's accuracy is affected by the properties of the scattering-parameters matrix as a function of a complex permittivity. In the majority of applications, the permittivity estimation is important, while the gain matrices $\mathbf{R}, \mathbf{T}$ are nuisance parameters; and the proposed method demonstrates stable and high permittivity estimation accuracy.

Additionally, we consider stochastic perturbations of the dielectric medium in the measurement domain and propose a heuristic approach to compensate the reduction in the method's performance caused by the perturbations. The stochastic perturbations manifest themselves in systematic permittivity-estimation and calibration errors. The proposed compensation approach introduces an averaging operator for observed samples of scattering-parameter observations, and noticeably improves estimation and calibration accuracies for moderate values of standard deviation of stochastic perturbations and high signal-to-noise ratio. At the low signal-to-noise levels, the simple arithmetic averaging performs well in both permittivity estimation and calibration accuracies.

ACKNOWLEDGEMENT

This work was supported by (i) the Swedish Governmental Agency for Innovation Systems (VINNOVA) under Grant 2016-00460 and (ii) Chalmers University of Technology. The computations were enabled by resources provided by Chalmers e-Commons at Chalmers.

REFERENCES

[1] Teppati, V., A. Ferrero, and M. Sayed, *Modern RF and Microwave Measurement Techniques*, Cambridge University Press, 2013.

[2] Fraden, J., *Handbook of Modern Sensors: Physics, Designs, and Applications*, Springer, 2004.

[3] Hislop, G., C. Craeye, and D. G. Ovejero, "Antenna calibration for near-field material characterization," *IEEE Transactions on Antennas and Propagation*, Vol. 64, No. 4, 1364–1372, Apr. 2016.

[4] Liu, Y., X. Xu, and G. Xu, "MIMO radar calibration and imagery for near-field scattering diagnosis," *IEEE Transactions on Aerospace and Electronic Systems*, Vol. 54, No. 1, 442–452, Feb. 2018.

[5] Zhao, W., C. Cheng, C. Yang, J. Xiao, Y. Wang, and Y. Huo, "Influence of non-ideal line-reflect-match calibration standards on vector network analyzer *S*-parameter measurements," *IET Science, Measurement & Technology*, Vol. 17, No. 6, 257–268, 2023.

[6] Lipor, J. and L. Balzano, "Robust blind calibration via total least squares," in *2014 IEEE International Conference on Acoustics, Speech and Signal Processing (ICASSP)*, 4244–4248, Florence, Italy, 2014.

[7] Bilen, Ç., G. Puy, R. Gribonval, and L. Daudet, "Convex optimization approaches for blind sensor calibration using sparsity," *IEEE Transactions on Signal Processing*, Vol. 62, No. 18, 4847–4856, 2014.

[8] Wei, Z., W. Wang, F. Dong, and P. Liu, "Self-calibration algorithm with gain-phase errors array for robust DOA estimation," *Progress In Electromagnetics Research M*, Vol. 99, 1–12, 2021.

[9] Yuan, B., Z. Jiang, J. Zhang, Y. Guo, and D. Wang, "Sparse self-calibration for microwave staring correlated imaging with random phase errors," *Progress In Electromagnetics Research C*, Vol. 105, 253–269, 2020.

[10] Ayestaran, R., J. A. Lopez-Fernandez, and F. L. H. Andres, "Self-calibration for fault or obstacle correction in continually rotating array antennas," *Progress In Electromagnetics Research*, Vol. 111, 365–380, 2011.

[11] Blakey, R. T., A. Mason, A. Al-Shamma'a, C. E. Rolph, and G. Bond, "Dielectric characterisation of lipid droplet suspensions using the small perturbation technique," in *Advancement in Sensing Technology: New Developments and Practical Applications*, 81–91, Springer-Verlag, Heidelberg, Germany, 2013.

[12] Korostynska, O., A. Mason, and A. Al-Shamma'a, "Microwave sensors for the non-invasive monitoring of industrial and medical applications," *Sensor Review*, Vol. 34, No. 2, 182–191, Mar. 2014.

[13] Stenmark, S., T. Rylander, and T. McKelvey, "Neural networks for the estimation of low-order statistical moments of a stochastic dielectric," in *2021 IEEE International Instrumentation and Measurement Technology Conference (I2MTC)*, 1–6, Glasgow, United Kingdom, May 2021.

[14] Andria, G., F. Attivissimo, A. D. Nisio, A. Trotta, S. M. Camporeale, and P. Pappalardi, "Design of a microwave sensor for measurement of water in fuel contamination," *Measurement*, Vol. 136, 74–81, Mar. 2019.

[15] Chen, L. F., C. K. Ong, C. P. Neo, V. V. Varadan, and V. K. Varadan, *Microwave Electronics: Measurement and Materials Characterization*, John Wiley & Sons, 2004.

[16] Buckmaster, H. A., "Precision microwave complex permittivity measurements of high loss liquids," *Journal of Electromagnetic Waves and Applications*, Vol. 4, No. 7, 645–659, 1990.

[17] Hasar, U. C. and O. Simsek, "A calibration-independent microwave method for position-insensitive and nonsingular dielectric measurements of solid materials," *Journal of Physics D: Applied Physics*, Vol. 42, No. 7, 075403, Mar. 2009.

[18] Wan, C., B. Nauwelaers, W. D. Raedt, and M. V. Rossum, "Two new measurement methods for explicit determination of complex permittivity," *IEEE Transactions on Microwave Theory and Techniques*, Vol. 46, No. 11, 1614–1619, Nov. 1998.

[19] Lanzi, L., M. Carlà, C. M. C. Gambi, and L. Lanzi, "Differential and double-differential dielectric spectroscopy to measure complex permittivity in transmission lines," *Review of Scientific Instruments*, Vol. 73, No. 8, 3085–3088, 2002.

[20] Hasar, U. C. and J. J. Barroso, "Electrical characterization of 3-D periodic microwire media using calibration-independent techniques," *Journal of Electromagnetic Waves and Applications*, Vol. 25, No. 14–15, 2110–2119, 2011.

[21] Xing, L., J. Zhu, Q. Xu, Y. Zhao, C. Song, and Y. Huang, "Generalised probe method to measure the liquid complex permittivity," *IET Microwaves, Antennas & Propagation*, Vol. 14, No. 8, 707–711, 2020.

[22] Nohlert, J., T. Rylander, and T. McKelvey, "Microwave measurement system for detection of dielectric objects in powders," *IEEE Transactions on Microwave Theory and Techniques*, Vol. 64, No. 11, 3851–3863, 2016.

[23] Winges, J., L. Cerullo, T. Rylander, T. McKelvey, and M. Viberg, "Compressed sensing for the detection and positioning of dielectric objects inside metal enclosures by means of microwave measurements," *IEEE Transactions on Microwave The-*

ory and Techniques, Vol. 66, No. 1, 462–476, 2018.

[24] Aster, R. C., B. Borchers, and C. H. Thurber, *Parameter Estimation and Inverse Problems*, 2nd ed., Academic Press, 2013.

[25] Engen, G. F. and C. A. Hoer, "Thru-reflect-line: An improved technique for calibrating the dual six-port automatic network analyzer," *IEEE Transactions on Microwave Theory and Techniques*, Vol. 27, No. 12, 987–993, 1979.

[26] Agilent Technologies, "Applying error correction to network analyzer measurements," Agilent AN 1287–3, 2002.

[27] Nicolson, A. M. and G. F. Ross, "Measurement of the intrinsic properties of materials by time-domain techniques," *IEEE Transactions on Instrumentation and Measurement*, Vol. 19, No. 4, 377–382, Nov. 1970.

[28] Weir, W. B., "Automatic measurement of complex dielectric constant and permeability at microwave frequencies," *Proceedings of the IEEE*, Vol. 62, No. 1, 33–36, 1974.

[29] Valagiannopoulos, C. A., "A novel methodology for estimating the permittivity of a specimen rod at low radio frequencies," *Journal of Electromagnetic Waves and Applications*, Vol. 24, No. 5–6, 631–640, 2010.

[30] Kress, R. and W. Rundell, "Inverse scattering for shape and impedance revisited," *Journal of Integral Equations and Applications*, Vol. 30, No. 2, 293–311, 2018.

[31] Balanis, C. A., *Antenna Theory: Analysis and Design*, John Wiley & Sons, 2016.

[32] Jaglan, N., B. Kanaujia, S. D. Gupta, and S. Srivastava, "Triple band notched UWB antenna design using electromagnetic band gap structures," *Progress In Electromagnetics Research C*, Vol. 66, 139–147, 2016.

[33] Koziel, S. and L. Leifsson, *Surrogate-Based Modeling and Optimization*, Springer, 2013.

[34] Jin, J., C. Zhang, F. Feng, W. Na, J. Ma, and Q.-J. Zhang, "Deep neural network technique for high-dimensional microwave modeling and applications to parameter extraction of microwave filters," *IEEE Transactions on Microwave Theory and Techniques*, Vol. 67, No. 10, 4140–4155, Oct. 2019.

[35] Sahu, K. C., S. Koziel, and A. Pietrenko-Dabrowska, "Surrogate modeling of passive microwave circuits using recurrent neural networks and domain confinement," *Scientific Reports*, Vol. 15, No. 1, 13322, Apr. 2025.

[36] Chávez-Hurtado, J. L. and J. E. Rayas-Sánchez, "Polynomial-based surrogate modeling of RF and microwave circuits in frequency domain exploiting the multinomial theorem," *IEEE Transactions on Microwave Theory and Techniques*, Vol. 64, No. 12, 4371–4381, Dec. 2016.

[37] Ardizzone, L., J. Kruse, S. Wirkert, D. Rahner, E. W. Pellegrini, R. S. Klessen, L. Maier-Hein, C. Rother, and U. Köthe, "Analyzing inverse problems with invertible neural networks," *ArXiv Preprint ArXiv:1808.04730*, Feb. 2019.

[38] Radev, S. T., U. K. Mertens, A. Voss, L. Ardizzone, and U. Köthe, "BayesFlow: Learning complex stochastic models with invertible neural networks," *IEEE Transactions on Neural Networks and Learning Systems*, Vol. 33, No. 4, 1452–1466, 2022.

[39] Valagiannopoulos, C., "On measuring the permittivity tensor of an anisotropic material from the transmission coefficients," *Progress In Electromagnetics Research B*, Vol. 9, 105–116, 2008.

[40] Nilsson, F., U. W. Gedde, and M. S. Hedenqvist, "Modelling the relative permittivity of anisotropic insulating composites," *Composites Science and Technology*, Vol. 71, No. 2, 216–221, 2011.